

EFFECTS OF TRANSPORT PROCESSES TO THE
DEPOSITION AND QUALITY OF ATMOSPHERIC
PRESSURE CHEMICAL VAPOUR DEPOSITED
GRAPHENE

BY

FATIN BAZILAH BINTI FAUZI

A thesis submitted in fulfilment of the requirement for the
degree of Doctor of Philosophy (Engineering)

Kulliyyah of Engineering
International Islamic University Malaysia

FEBRUARY 2021

ABSTRACT

Until now, producing homogeneous chemical vapour deposited graphene with zero defects remains a challenge. The research on chemical aspects has been extensively explored either through experiments or computational studies. Given that it is a mass-transport limited process for atmospheric-pressure CVD (APCVD), the gas-phase dynamics and interfacial phenomena at the gas-solid interface (i.e., the boundary layer) is a crucial controlling factors. In this research, the importance of CVD fluid dynamics aspect was emphasised through fundamental studies at both gas-phase and gas-solid phase. As a preliminary study, an extensive review of available APCVD literature provided information on the relationship of graphene quality and its corresponding growth parameter. From these parameters, Reynolds number was calculated with the consideration that it is a ternary gas mixture. This was then compiled into a CH₄-H₂-Ar ternary plot which predicts the quality of graphene and Reynolds number at all gas compositions. Higher Reynolds number was found to be promising for high-quality graphene deposit which could be obtained at the gas composition range of $\leq 1\%$ of CH₄, $\leq 10\%$ of H₂, and $\geq 90\%$ of Ar. Following this, a customised homogenous gas with properties similar to mixture of CH₄, H₂ and Ar was used in our computational fluid dynamics (CFD) of APCVD graphene. The in-depth details on gas-phase dynamics, interfacial phenomena, particularly the boundary layer and mass transport during the deposition process, were studied. Conditions, where gravity parameter is vital or could be safely neglected in CFD, was also determined. CFD model also allowed a close-up view of the boundary layer at the gas-solid interface. This was found to provide the most reasonable estimation of boundary-layer thickness formed on top of substrate for a bounded flow system like in a CVD. Higher Reynolds number formed thinner boundary layer. Consecutively, the relationship between the deposited graphene quality with Reynolds number, boundary-layer thickness and mass transport were explored. Calculated mass transport coefficient shows a good correlation to graphene thickness but not it's defect density which suggests that graphene defects are more dependent on factors other than fluid dynamics. At the highest Reynolds number of 84, few-layer graphene with monolayer ratio, I_{2D}/I_G of ~ 0.67 and defect ratio, I_D/I_G of ~ 0.45 was obtained. Wherein the quality of graphene improves when the I_D/I_G decreased by 90% and I_{2D}/I_G increased by 60%. Based on the experimental and computational studies, transport process was shown to have a vital role in the APCVD graphene growth.

خلاصة البحث

لا يزال إنتاج بخار كيميائي متجانس غير معيوب من الجرافين المترسب تحديًا حتى يومنا هذا. تم القيام بالعديد من الأبحاث في الجوانب الكيميائية على نطاق واسع إما من خلال التجارب أو الدراسات الحاسوبية. بالنظر إلى أنها عملية نقل جماعي محدودة للضغط الجوي (CVD) (APCVD)، فإن ديناميكيات الطور الغازي والظواهر البينية في السطح البيني الغازي الصلب (أي الطبقة الفاصلة) هي عوامل التحكم الحاسمة. تم التأكيد على أهمية ديناميكيات APCVD من خلال الدراسات الأساسية في كل من المرحلة الغازية والمرحلة الغازية الصلبة في هذا البحث. كدراسة أولية، قدمت مراجعة شاملة لأدبيات APCVD المتاحة معلومات حول العلاقة بين جودة الجرافين وعامل النمو المقابل لها. من بين هذه العوامل، تم حساب رقم رينولدز مع الأخذ في الاعتبار أنه خليط غازي ثلاثي. تم جمعه بعد ذلك في مخطط CH_4 - H_2 -Ar الثلاثي والذي يتوقع جودة الجرافين ورقم رينولدز في جميع التركيبات الغازية. تم التوصل إلى أن أرقام رينولدز العالية تُعد واعدة بنسبة للجودة العالية لرواسب الجرافين والتي يمكن الحصول عليها في نطاق تكوين الغاز الذي يبلغ أقل من 1% من CH_4 ، و 10% من H_2 ، و 90% من Ar. بعد ذلك، تم تطوير نموذج غاز متجانس مخصص بشكل أكبر لديناميات السوائل الحاسوبية (CFD) من جرافين APCVD. تمت دراسة التفاصيل المتعمقة حول ديناميكيات الطور الغازي والظواهر البينية، خاصة الطبقة الفاصلة والنقل الجماعي أثناء عملية الترسيب. تم أيضًا تحديد الظروف التي تكون فيها عوامل الجاذبية أمرًا حيويًا أو يمكن إهمالها بدون عواقب في CFD. يسمح نموذج CFD أيضًا برؤية قريبة للطبقة الفاصلة في السطح البيني الغاز الصلب. تم العثور على هذا لتوفير أكثر تقدير منطقي لسُمك الطبقة الفاصلة لنظام تدفق محدود كما هو الحال في CVD. تم إثبات عدم صحة التقدير التقريبي الآخر المعتمد على نموذج Blasius. شكل رقم رينولدز الأعلى طبقة حد أقل سمكًا. وتم استكشاف العلاقة بين الجرافين المترسب ورقم رينولدز وسمك الطبقة الفاصلة والنقل الجماعي. يُظهر عامل النقل الجماعي المحسوب ارتباطًا جيدًا بسمك الجرافين ولكن لا يُشير إلى كتابة معيوبة، والذي يشير إلى أن عيوب الجرافين تعتمد بشكل أكبر على عوامل أخرى غير ديناميكيات السوائل. أثناء تطبيق أعلى رقم رينولدز (البالغ 84)، تم الحصول على عدد قليل من الجرافين مع نسبة أحادية الطبقة I_{2D}/I_G بقيمة ~ 0.67 ونسبة العيوب $I_D/I_G \sim 0.45$. تحسنت جودة الجرافين عند انخفاض I_D/I_G بنسبة 90% وزادت I_{2D}/I_G بنسبة 60%. بناءً على الدراسات التجريبية والحاسوبية، تبين أن لعملية النقل دور حيوي في نمو جرافين APCVD.

APPROVAL PAGE

The thesis of Fatin Bazilah Binti Fauzi has been approved by the following:



Mohd Hanafi Bin Ani
Supervisor



Syed Noh Bin Syed Abu Bakar
Co-Supervisor

Waqar Asrar
Internal Examiner

Azrul Azlan Bin Hamzah
External Examiner

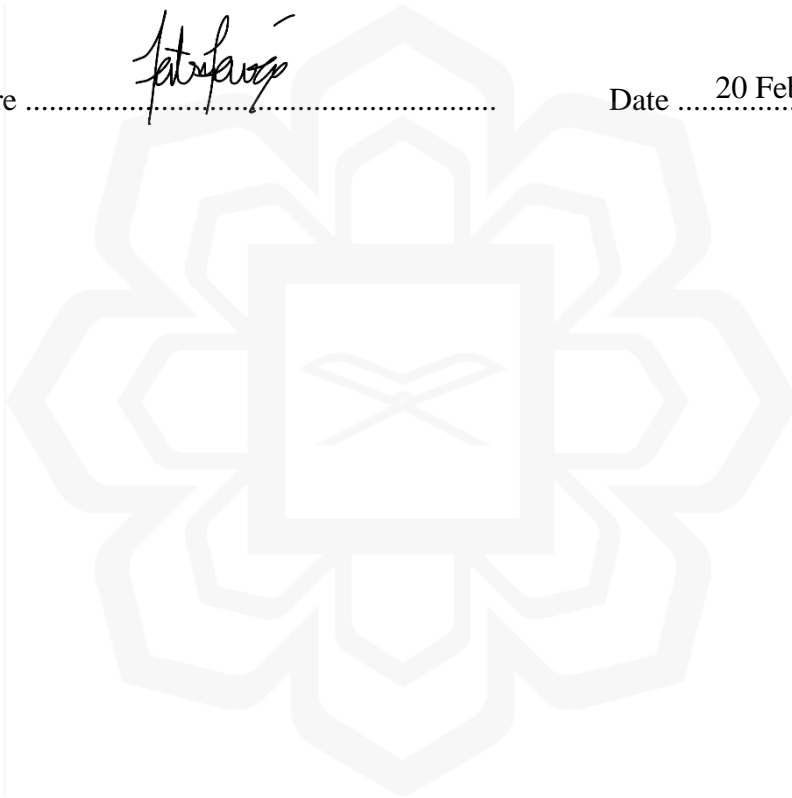
Akram Zeki Khedher
Chairman

DECLARATION

I hereby declare that this thesis is the result of my own investigations, except where otherwise stated. I also declare that it has not been previously or concurrently submitted as a whole for any other degrees at IIUM or other institutions.

Fatin Bazilah Binti Fauzi

Signature  Date 20 February 2021



INTERNATIONAL ISLAMIC UNIVERSITY MALAYSIA

**DECLARATION OF COPYRIGHT AND AFFIRMATION OF
FAIR USE OF UNPUBLISHED RESEARCH**

**EFFECTS OF TRANSPORT PROCESSES TO THE
DEPOSITION AND QUALITY OF ATMOSPHERIC PRESSURE
CHEMICAL VAPOUR DEPOSITED GRAPHENE**

I declare that the copyright holders of this thesis are jointly owned by the student and IIUM.


Copyright © 2021 Fatim Bazilah Binti Fauzi and International Islamic University Malaysia. All rights reserved.

No part of this unpublished research may be reproduced, stored in a retrieval system, or transmitted, in any form or by any means, electronic, mechanical, photocopying, recording or otherwise without prior written permission of the copyright holder except as provided below

1. Any material contained in or derived from this unpublished research may be used by others in their writing with due acknowledgement.
2. IIUM or its library will have the right to make and transmit copies (print or electronic) for institutional and academic purposes.
3. The IIUM library will have the right to make, store in a retrieved system and supply copies of this unpublished research if requested by other universities and research libraries.

By signing this form, I acknowledged that I have read and understand the IIUM Intellectual Property Right and Commercialisation policy.

Affirmed by Fatim Bazilah Binti Fauzi


.....

Signature

20 February 2021
.....

Date

ACKNOWLEDGEMENTS

*In the name of Allah, Most Gracious, Most Merciful.
May the blessing and peace of Allah be upon our Prophet Sayyidina Muhammad ibn
Abdullah (peace be upon him), and upon his families, his companions and all his
godly followers.*

Alhamdulillah and praise to Allah SWT for being able to finish my studies. First of all, I would like to give my special thanks to my honourable supervisor, Dr Mohd Hanafi Bin Ani for his countless guidance and advice throughout my study. This also goes to my co-supervisor with my field-supervisor, Dr Syed Noh Syed Abu Bakar and Dr Mohd Ambri Mohamed.

I would like to express my gratitude to my colleagues (Edhuan Bin Ismail, Mukhtaruddin Bin Musa, Mohd Shukri Bin Sirat) and the members of Corrosion Lab 2 for their help and friendly support. Many thanks to IIUM laboratory staffs in Kulliyah of Engineering especially Br. Ibrahim (SEM laboratory), UPNM and UKM laboratory staffs for their help and expertise.

I would also like to thank the Ministry of Higher Education (MOHE) for Long-term Research Grant Scheme (LRGS15-003-0004) and IIUM for their funding and facilities.

The constant encouragement from my parents and my family as a continued source of inspiration is like a breath of fresh air every time I needed it. Their faith in me pushed me to be the best, to explore this learning path and to pursue my dream. For that, I am eternally grateful.

Thank you very much.

TABLE OF CONTENTS

Abstract	ii
Abstract in Arabic	iii
Approval Page	iv
Declaration	v
Copyright	vi
Acknowledgements	vii
Table of Contents	viii
List of Tables	xi
List of Figures	xii
List of Abbreviations	xvii
List of Symbols	xviii
CHAPTER ONE: INTRODUCTION	1
1.1 Study Background	1
1.1.1 Properties and Production of Graphene	1
1.1.2 CVD	5
1.1.3 Fluid Dynamics in CVD	7
1.1.4 CFD	9
1.2 Research Scope	10
1.3 Problem Statements	10
1.4 Research Philosophy	12
1.5 Research Objectives	13
1.6 Thesis Structure	14
CHAPTER TWO: LITERATURE REVIEW	16
2.1 Introduction	16
2.2 Overview of Fluid Dynamics in CVD	16
2.3 Dimensionless numbers related to the conventional CVD process	20
2.4 CFD Works of CVD	25
2.4.1 Modifications on Reactor Geometry	28
2.5 Experimental Works	38
2.5.1 Flow Field Characterization	38
2.6 Gas-Solid Phase	41
2.6.1 Boundary Layer Formation	41
2.6.2 Mass Transport of Active Species through the Boundary Layer	42
2.7 Summary	46
CHAPTER THREE: METHODOLOGY	48
3.1 Introduction	48
3.2 Reynolds Number	49
3.3 CFD	52
3.3.1 Modelling of CVD Reactor	53
3.3.2 Computational Domain, Mesh Numerical Arrangement Setup and Boundary Conditions	54

3.3.3 Homogenous Gas Mixture Properties	57
3.4 Boundary-Layer Thickness.....	59
3.4.1 Calculated Boundary-Layer Thickness	59
3.4.2 Estimation of Boundary-Layer Thickness on the Substrate Through CFD.....	59
3.5 Mass Transport, Residence Time, and Diffusion Time	60
3.6 Experimentation: APCVD	63
3.6.1 Furnace Calibration.....	64
3.6.2 Sample Preparation	64
3.6.3 Pre-Annealing	65
3.6.4 Deposition	65
3.6.5 Transfer Process	68
3.6.6 Characterisation	68
3.6.7 Data Analyses	69
3.7 Summary.....	70
CHAPTER FOUR: OPTIMISATION OF GAS COMPOSITION AND PARAMETRIC STUDY ON APCVD GRAPHENE.....	71
4.1 Introduction.....	71
4.2 Optimisation of the Gas Composition From Literature Based on Reynolds Number	72
4.2.1 Effects of Gas Composition on the Reynolds Number	74
4.2.2 Effects of Reynolds Number on the Graphene Quality and Growth	77
4.3 Parametric Study on APCVD Graphene	78
4.3.1 Substrate Pre-Annealing	79
4.3.2 CH ₄ Concentration for APCVD Deposition	83
4.4 Summary.....	86
CHAPTER FIVE: RESULTS AND DISCUSSIONS.....	87
5.1 Part 1: CFD of APCVD, Boundary-Layer Thickness and Mass Transport.....	87
5.1.1 Introduction.....	87
5.1.2 Gas Flow Temperature and Velocity Distribution of APCVD	88
5.1.2.1 Temperature Distributions.....	88
5.1.2.2 Velocity Distributions.....	90
5.1.3 Effects of Reynolds Number on the Boundary-Layer Thickness	92
5.1.4 Effects of Reynolds Number and Boundary-Layer Thickness towards the Mass Transport, Residence Time and Diffusion Time.....	95
5.1.5 Effects of Substrate's Placement on the Boundary-Layer Thickness	99
5.2 Part 2: APCVD Graphene with Characterisations and its Correlation with Fluid Dynamics, Mass Transport Studies.....	102
5.2.1 Introduction.....	102
5.2.2 Characterisations	102
5.2.3 Correlation Between Reynolds Number, Boundary-Layer Thickness and Mass Transport with Graphene Quality.....	107

5.2.4 Effects of Substrate's Placement toward Graphene Quality	111
5.3 Summary	112
CHAPTER SIX: CONCLUSIONS AND RECOMMENDATIONS	114
REFERENCES.....	118
LIST OF PUBLICATIONS AND CONFERENCES.....	127
APPENDIX I: EXCEL CALCULATOR.....	129
APPENDIX II: COMPUTATIONAL FLUID DYNAMICS ANALYSIS FOR PRESENT CVD TUBE	130
APPENDIX III: DATA AND INPUTS OF ANSYS WORKBENCH	145
APPENDIX IV: BASIC STEPS OF ANSYS WORKBENCH.....	152



LIST OF TABLES

Table 2-1	A non-comprehensive list of experimental parameters that influence important fluid dynamics parameters of the CVD reactor.	19
Table 2-2	Established dimensionless numbers in fluid dynamics applicable for a CVD reactor with the definition, field of use, and typical values obtained for LPCVD and APCVD.	21
Table 2-3	Modification and experimental conditions for graphene deposition in the literature, showing the reaction temperature (T), pressure (P), and composition of CH_4 , H_2 , Ar in the volumetric flow rate (Q) with the graphene quality.	37
Table 3-1	Literature used for the Reynolds number calculation of horizontal hot-walled tubular APCVD of graphene. The numbers here index the references displayed in Figure 4.1.	52
Table 3-2	List of inlet velocities used in the CFD.	56
Table 3-3	Numerical setups of the CFD code used.	56
Table 3-4	Polynomial equation constants for a homogeneous gas mixture of 0.01 atm CH_4 :0.05 atm H_2 :0.94 atm Ar used in the CFD setup.	58
Table 3-5	List of experiments of various gas composition using a different type of CH_4 concentrations for APCVD of graphene using Cu catalyst.	67
Table 3-6	The details on the materials used in this APCVD.	69
Table 4-1	Gas properties of CH_4 , H_2 , and Ar at 1273 ± 100 K.	75
Table 4-2	The summary annealing process for graphene growth by APCVD from literature.	80
Table 5-1	Mass transport coefficient, h_g and deposition rate, R_D at different total volumetric flow rate, Q_T .	96

LIST OF FIGURES

Figure 1.1	Structures of carbon allotropes in all dimensions (Oganov et al., 2013).	2
Figure 1.2	Graphene production in terms of methods, cost and quality (Novoselov et al., 2012).	5
Figure 1.3	The schematic diagram of a typical tube-furnace CVD system (Miao et al., 2011).	6
Figure 1.4	A simplified schematic diagram of graphene growth on a Cu substrate from CH ₄ gas (Ani et al., 2018).	6
Figure 1.5	Inter-relation of important experimental factors that influence both chemical reactions and fluid dynamics (grey box) in the CVD method. Adapted from Kleijn et al. (2007).	8
Figure 2.1	Gas velocity magnitude and direction on a plane 10 mm above the wafer surface (Pitney and Kommu, 2008).	17
Figure 2.2	Variation of deposition morphology with carrier gas composition: (a) 1000 sccm H ₂ , 0 sccm Ar; (b) 800 sccm H ₂ , 200 sccm Ar; (c) 500 sccm H ₂ , 500 sccm Ar; (d) 200 sccm H ₂ , 800 sccm Ar; (e) 0 sccm H ₂ , 1000 sccm Ar (Dirkx and Spear, 1984).	18
Figure 2.3	(a) Vertical cylinder reactor, (b) variation of the gas temperature with position along with the susceptor, and (c) comparison of the growth rate variation predicted by the constant temperature modes (dashed lines) and developing temperature modes (solid lines) (Manke, 1977).	24
Figure 2.4	Contours of (a) temperature, T ; (b) velocity, v ; and (c) molar concentration of CH ₄ distribution on the symmetry plane at different pressures (Li, Huang, et al., 2015).	28
Figure 2.5	Schematic diagram of (a) circumfluent CVD system, (b) CFD of gas flow streamlined in the inner tube, (c) Cu substrate after the reaction, (d) OM images of graphene domain at three different spots along the reactor, and (e) fluid field velocity distribution in the inner tube (Wang et al., 2015).	30
Figure 2.6	(a) The influence of H ₂ and CH ₄ gas concentrations on the nucleation density, (b) increase in the grain size of graphene using a restricted chamber, and (c) partial pressure of CH ₄ and H ₂ inside the furnace tube with a cuvette (Song et al., 2015).	32

Figure 2.7	(a) Schematic diagram of LPCVD with one open end confined space with opposite gas flow direction, (b) velocity distributions of the gas flow, (c) velocity distribution of the reactant, (d) concentration distribution of the reactant and effects of H ₂ concentration on the nucleation density (e) in a 60 min annealing time, (f) in a 30 min annealing time (Chen et al., 2015).	33
Figure 2.8	Gas flow in (a) conventional CVD, (b) slower gas flow after a diffuser, and (c) a slower and circumfluent gas flow created with the addition of a backwards-facing restricted chamber.	35
Figure 2.9	Figure 2.9 Optical-based fluid characterisation (a) N ₂ and Ar, medium flow velocities $4 \leq v \leq 0.1 \text{ m s}^{-1}$. Temperature = 1350 K, susceptor length = 20 cm, (b) H ₂ and He, all flow velocities 0.9 m s^{-1} . Temperature = 1148 K, susceptor length = 20 cm (Giling, 1982), (c) Transition from laminar to turbulent flow conditions as determined by LLS intensity measurements (Woods et al., 2004).	40
Figure 2.10	Simple schematic representation of the metal-organic CVD mechanism (Ritala et al., 2009).	42
Figure 2.11	(a) Processes involved during graphene synthesis using low carbon solid solubility catalysts of Cu in a CVD process and (b) mass transport and surface reaction fluxes under steady-state conditions (Bhaviripudi et al., 2010).	43
Figure 2.12	Schematic of boundary layer above Cu foil. The Cu foil substrate surface is parallel (a) and tilted (b) to the bulk gas flow; OM images of large-area graphene film grown on a parallel substrate (c) and grown on a tilted substrate (d); SEM images of graphene grain distribution on Cu foil substrate grown with the substrate parallel to the gas flow (e), (e1) and (e2) and tilted to the bulk gas flow (f), (f1) and (f2) (Zhang et al., 2012).	45
Figure 3.1	Overall flow chart of the research.	48
Figure 3.2	Schematic of the 2D-CVD model with 30 μm Cu substrate placed flat within the isothermal zone (shaded region). Unit: cm.	53
Figure 3.3	Meshing arrangement along the (a) wall and (b) furnace area.	54
Figure 3.4	(a) Schematic of the five lines drawn on the flat Cu substrate, (b) velocity profile of each line on flat Cu substrate from CFD, (c) schematic of the five lines drawn on the inclined Cu substrate and (d) velocity profile of each line on inclined Cu substrate from CFD.	60

Figure 3.5	Schematic diagram of the experimental APCVD setup.	64
Figure 3.6	Summary of the APCVD–graphene synthesis process with times, temperatures and gases used.	67
Figure 3.7	The transfer process of deposited graphene on Cu to the appropriate substrates for characterisations.	68
Figure 4.1	Calculated Reynolds numbers for horizontal hot-walled tubular APCVD of graphene as reported in the literature (Table 3-1). Note that the conditions only for 1273 ± 100 K on a Cu substrate with various gas compositions.	73
Figure 4.2	Ternary contour plot of the Reynolds number showing the effect of the gas composition at an arbitrary temperature and total flow rate, plotted together with the reported gas composition of CH_4 , H_2 and Ar in the literature (Table 3-1). Note that the total gas composition for all gases is 1.	76
Figure 4.3	(a) Graphene quality for APCVD hot walled furnace versus the gas composition of CH_4 , H_2 and Ar on Cu at 1273 ± 100 K as reported in the literature (Table 3-1), (b) enlarged CH_4 -rich region (red) and (c) H_2 -rich region (blue). Note that the total gas composition for all gases is 1.	77
Figure 4.4	6×10 stitched surface morphology of $1 \text{ cm} \times 1 \text{ cm}$ Cu substrate after annealing at 100 sccm H_2 for 240 min by (a) fast cooling and (b) slow cooling.	81
Figure 4.5	Effects of annealing time towards the Cu grain size.	82
Figure 4.6	6×10 stitched surface morphology of $1 \text{ cm} \times 1 \text{ cm}$ $30 \mu\text{m}$ Cu substrate after annealing for 240 min at (a) 1273 K and (b) 1173 K.	83
Figure 4.7	Raman spectra of deposited thin film using 5 ppm and 19 ppm CH_4 .	84
Figure 4.8	SEM images of the deposited thin film at two different spots (a) 2k magnification and (b) 2.3k magnification and (c) 4k magnification. Sample of 240 min deposition time using 19 ppm CH_4 .	84
Figure 4.9	Raman spectra for deposited thin films of 1% CH_4 concentration with different deposition time at (a) 3 min and (b) 5 min.	85
Figure 5.1	The contour of temperature distribution on the APCVD at 1273 K with different Reynolds numbers (a) with and (b) without gravitational effects. Y-axis is exaggerated for clarity.	89

Figure 5.2	The contour of velocity distribution on the APCVD at 1273 K with different Reynolds numbers (a) with and (b) without gravitational effects. Y-axis is exaggerated for clarity.	91
Figure 5.3	(a) The velocity profile of each line on the CFD velocity contour and (b) variation of boundary-layer thickness along the Cu substrate length of 1.5 cm at Reynolds number of 67.	93
Figure 5.4	Boundary-layer thickness formed on the Cu substrate inside of the APCVD from CFD (a) with and without gravitational effects and (b) as calculated using Eq. (3.13). Grey dotted horizontal line: tube radius.	94
Figure 5.5	Effects of the Reynolds number towards the (a) mass transport coefficient, (b) deposition rate and boundary-layer thickness towards the (c) mass transport coefficient, (d) deposition rate.	97
Figure 5.6	Schematic of the process involved in the near-surface conditions of the APCVD model. CH_x (g) = active carbon species and intermediates; C (s) = carbon solid; H_2 (g) = by-products H_2 gas.	98
Figure 5.7	Relationship between Reynolds number to the residence time and diffusion time.	99
Figure 5.8	(a) The velocity profile of each line on the CFD velocity distribution and (b) variation of boundary-layer thickness along the inclined Cu substrate at Reynolds number of 67.	100
Figure 5.9	Comparison of the boundary-layer thickness formed along the Cu substrate length (flat and inclined) in APCVD.	101
Figure 5.10	Boundary-layer thickness formed on the (a) inclined Cu substrate and (b) flat Cu substrate inside the APCVD.	102
Figure 5.11	Raman spectra of the graphene deposited at different Reynolds number varies from 8 to 84 with D, G and 2D peaks.	103
Figure 5.12	(a)-(b) TEM images of deposited graphene at Reynolds number of 67 on TEM lacey carbon grid at 1 μm and 200 nm scale with dark spots (red dotted circle) of PMMA residues on top, (c) SAED pattern of a few-layer graphene characteristic for a hexagonal lattice and (d) Raman spectra for the deposited graphene.	104
Figure 5.13	(a) AFM image of a deposited graphene flake on a quartz substrate and (b) height profile of the graphene flake along the red dotted line in (a).	105

Figure 5.14	(a) HRTEM image with intensity profile plot along the red line (inset) and (b) inter-planar distance of few-layer graphene indicate by yellow arrows (inset: FFT image).	105
Figure 5.15	SEM images of graphene grown at 3 different spots of front, centre, and rear. Reynolds number varies from 8 to 67 (Scale bar: 10 μm).	106
Figure 5.16	Effects of the Reynolds number towards the (a) monolayer ratio of I_{2D}/I_G , (b) defect ratio of I_D/I_G and reciprocal of boundary-layer thickness towards (c) monolayer ratio of I_{2D}/I_G , (d) defect ratio of I_D/I_G .	108
Figure 5.17	Effects of mass transport coefficient towards monolayer ratio of I_{2D}/I_G .	109
Figure 5.18	Effects of the residence time towards the (a) monolayer ratio of I_{2D}/I_G , (b) defects ratio of I_D/I_G and effects of the diffusion time towards the (c) monolayer ratio of I_{2D}/I_G , (d) defects ratio of I_D/I_G .	110
Figure 5.19	Effects of Reynolds number to graphene quality on the (a) inclined and (b) flat placement of Cu substrate.	112

LIST OF ABBREVIATIONS

0D	Zero-Dimensional
1D	One-Dimensional
2D	Two-Dimensional
3D	Three-Dimensional
AFM	Atomic Force Microscope
AP	Atmospheric Pressure
APCVD	Atmospheric-Pressure CVD
ASTM	American Society for Testing and Materials
CFD	Computational Fluid Dynamics
CNT	Carbon Nanotube
CVD	Chemical Vapour Deposition
Eq.	Equation
LP	Low Pressure
LPCVD	Low-Pressure CVD
MFC	Mass Flow Controller
OM	Optical Microscope
PMMA	Polymethyl Methacrylate
ppm	parts per million
RF	Radio Frequency
rpm	revolutions per minute
SAED	Selected Area Electron Diffraction
sccm	standard cubic centimetre per minute
SEM	Scanning Electron Microscope
STP	Standard Pressure and Temperature
TC	Thermocouple
TEM	Transmission Electron Microscope
UHVCVD	Ultrahigh-Vacuum CVD

LIST OF SYMBOLS

Å	Angstrom
Ar	Argon
atm	Atmosphere
BCl ₃	Boron trichloride
C	Carbon
CH ₄	Methane
cm	Centimetre
cm ⁻¹	Wavenumber
Cu	Copper
D	Tube diameter
FeCl ₃	Iron chloride (III)
GPa	Gigapascal
Gr	Grashof number
H ₂	Hydrogen gas
He	Helium gas
K	Kelvin
k	Kilo
kg	Kilogram
Kn	Knudsen number
L	Tube length
M	Molar
m	Meter
min	Minute
mm	Millimetre
mm ²	Millimetre squared
N ₂	Nitrogen gas
P	Pressure

Pa	Pascal
Q	Volumetric flow rate
r	Radius
Re	Reynolds number
S	Siemens
s	Second
SiB ₄	Silicon boride
SiH ₄	Silane
sq	Square
T	Temperature
TPa	Terapascal
V	Volt
W	Watt
ZnO	Zinc oxide
δ	Boundary-layer thickness
μ	Viscosity
μm	Micrometre
π	Pi (3.14159265359)
ρ	Density
Ω	Ohm

CHAPTER ONE

INTRODUCTION

This chapter provides the research background starting from the significance of graphene, its production method and the challenges in the production of high-quality large-area graphene that is currently the obstacle to its widespread use. With the current status of graphene research introduced, a vital point in the production process which is fluid dynamics is discussed. From there, issues in this field of study will be highlighted and the objectives of this research are stated.

1.1 STUDY BACKGROUND

1.1.1 Properties and Production of Graphene

Carbon-based material was recently discovered to have extraordinary properties for various applications. Fabrication of carbon materials especially graphene, also known as ‘wonder material’, have gained massive research interest in a short duration due to its spectacular structural and electronic properties. Graphene is a 2D material made of a single atomic layer of graphite consisting of sp^2 carbon atoms in hexagonal lattices. It is the basic building block for other graphitic materials in other dimensions. Graphite is composed of a stack of many graphene layers forming a 3D structure; CNT is graphene in a tubular shape forming a 1D structure; fullerene is graphene in a spherical shape with some hexagonal lattices replaced by pentagon lattices forming a 0D structure. In contrast, sp^3 carbons form 3D carbon allotropes as diamonds and supercubane tetrahedral, BC8. Figure 1.1 shows the structures of all graphitic materials in all

dimensions and graphene is the basic structure with a single atom thick carbon layer (Oganov, Hemley, Hazen, and Jones, 2013).

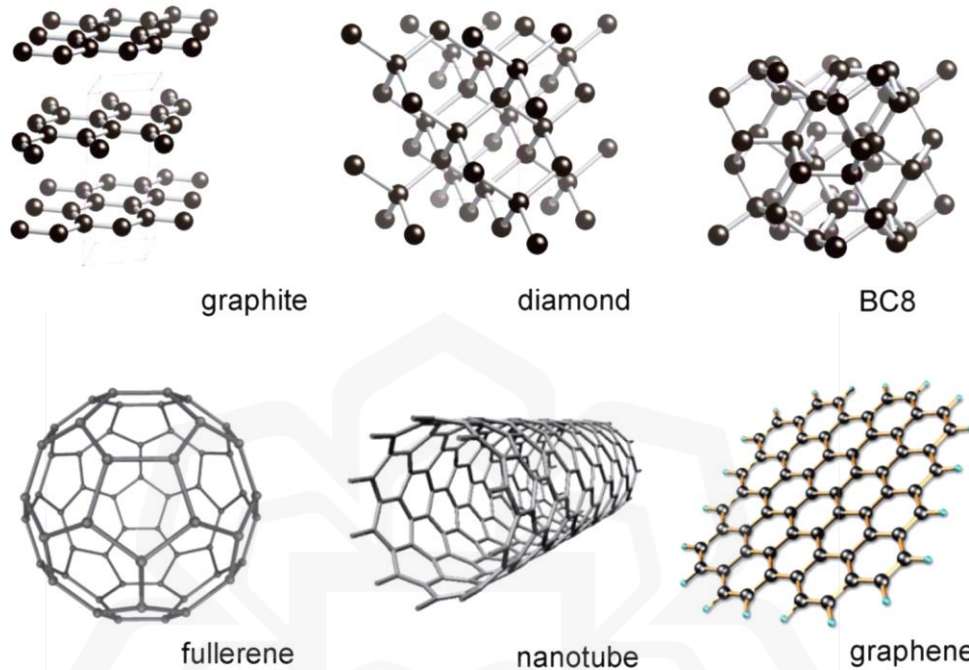


Figure 1.1 Structures of carbon allotropes in all dimensions (Oganov et al., 2013).

Theoretically, graphene has been studied for about sixty years and its superior characteristics beyond other materials' characteristics were discovered forty years later. Since 2004, graphene has gained massive interest with many applications relying on its superior properties and strength. Geim and Nosolev from Manchester University first discovered it that awarded them the Nobel Prize. It has become a reference for describing properties of other carbon allotropes (Geim and Novoselov, 2007).

Composed of carbons in sp^2 -hybridised bonds, it forms benzene rings with delocalised electron clouds. The sp^2 bonds provide excellent structural strength and fracture strength of ~ 1 TPa Young's modulus and 130 GPa, respectively (Lee, Wei, Kysar, and Hone, 2008). As a comparison, iron only has Young's modulus of 211 GPa.

Its delocalised π -electron clouds give rise to its conductivity. Its bulk conductivity is $0.96 \times 10^6 \Omega^{-1} \text{ cm}^{-1}$, higher than Cu which is $0.60 \times 10^6 \Omega^{-1} \text{ cm}^{-1}$. Graphene is the thinnest material ($\sim 3.35 \text{ \AA}$) with remarkable properties such as high electron mobility at room temperature ($\sim 2\text{--}2.5 \times 10^5 \text{ cm}^2 \text{ V}^{-1} \text{ s}^{-1}$), high optical transmissivity (2.3%), exceptional thermal conductivity ($4800\text{--}5300 \text{ W m}^{-1} \text{ K}^{-1}$) and high electrical conductivity (2000 S cm^{-1}) (Mayorov et al., 2011). Compared to conventional conductive materials such as metals and semiconductors, single-layer graphene possesses a sheet resistivity of $31 \Omega \text{ sq}^{-1}$ while maintaining its transparency and flexibility. Single-layer graphene was found to allow 98 % of visible light to pass through it (Zhao et al., 2014). Due to its benzene-like structure, pristine graphene is chemically inert giving chemical stability in a wide range of conditions.

No other materials can beat the superior characteristics of graphene. These particular properties of graphene have generated lots of interest and have been explored for more than fifty years. All the above properties are the reason why graphene is known as a ‘wonder material’. These characteristics give graphene the potential ability to be used in many fields of applications including optoelectronics, flexible solar cell, bio-sensing, nanocomposites, and energy storage devices (Ani et al., 2018; Azam et al., 2017; Mishra, Boeckl, Motta, and Iacopi, 2016). However, such characteristics only apply to high-quality graphene. Until now, it is still a challenge to produce high-quality large-area graphene consistently.

Currently, many methods have been developed to synthesise graphene in various dimensions, shapes, and quality (Novoselov et al., 2012). These methods can be categorised into bottom-up or top-down approaches. The top-down approach is the process where the hexagonal lattice graphene sheets are split from its large carbon building structures such as graphite and CNT. Meanwhile, a bottom-up approach is a

process building up new carbon hexagonal lattice of graphene from carbon precursors such as hydrocarbon molecules (Tour, 2014; Yi and Shen, 2015).

The interest in graphene spiked since the first successful mechanical exfoliation of monolayer graphene was reported by Novoselov and Geim in 2004 (Novoselov et al., 2004). This method is essentially a top-down approach. Since then, researches on graphene productions have been widely explored resulting in many new methods as shown in Figure 1.2 which sorts each method in terms of quality and cost for mass production (Novoselov et al., 2012). The highest quality of graphene can be produced using mechanical exfoliation, but this method is costly for mass production and produces only flakes. This method is only used for research purposes.

Meanwhile, liquid exfoliation is a method to produce graphene on a large scale with the cheapest production cost. But through this method, the poorest quality of graphene was produced. Graphene that was produced thus were unable to be used in nanoelectronics applications. Alternatively, growth on silicon carbide, CVD and molecular assembly has produced good quality graphene for nanoelectronics applications.

CVD has become the most favourable method for graphene production in terms of cost and quality compared to other methods. It can produce high-quality graphene with small defects (Zhang et al., 2013). Furthermore, CVD is well-known for its simplicity, scalability, large size of continuous graphene sheets, and reasonable material quality (Vlassiuk, Fulvio, et al., 2013). In addition, modifications of the CVD reactor, such as plasma-enhanced CVD (Braeuninger-Weimer, Brennan, Pollard, and Hofmann, 2016; Jacob et al., 2015) or flame deposition CVD (Ismail et al., 2017; Memon et al., 2011), have also been reported for graphene production. Due to the above reasons, rapid CVD graphene research is predicted to continue for the next few decades.

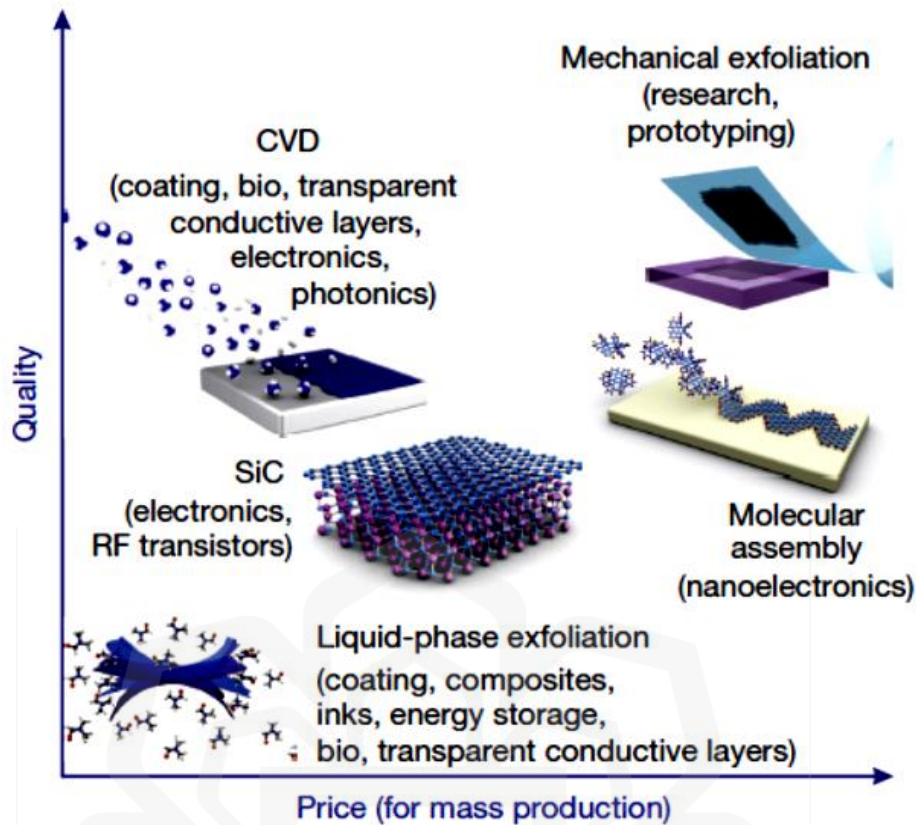


Figure 1.2 Graphene production in terms of methods, cost and quality (Novoselov et al., 2012).

1.1.2 CVD

The use of CVD for graphene production is not a new finding. It is a bottom-up approach where graphene will be deposited on the substrate through chemical reactions of the hydrocarbon species at a temperature range of 573 K to approximately 1273 K. Figure 1.3 shows the schematic diagram of a typical tube-furnace CVD system (Miao, Zheng, Liang, and Xie, 2011).

Carbon sources usually used for graphene deposition comes from hydrocarbons such as ethylene, methane, benzene, ethanol as well as polymers in any particular form but mostly in the gas form (Li et al., 2011; Yao et al., 2011). The gases that enter the reactor will be controlled by MFC, then the reaction will take place at the reactor where the substrate will be placed within it. The reaction can be any pressure condition. The